48th AIAA Aerospace Sciences Meeting Including the New Horizons Forum and Aerospace Exposition
4 - 7 January 2010, Orlando, Florida

AIAA 2010-724

The Numerical Simulation of Flapping Wings at Low Reynolds Numbers

Per-Olof Persson*
University of California, Berkeley, Berkeley, CA 94720-3840, U.S.A.

David J. Willis†
University of Massachusetts, Lowell, Lowell, MA 01854, U.S.A.

Jaime Peraire‡
Massachusetts Institute of Technology, Cambridge, MA 02139, U.S.A.

Although there are many examples of successful flapping flight in nature, the design of efficient flapping wings for human designed vehicles has been an elusive goal. One of the main obstacles encountered is the multi-dimensional design space. In order to efficiently search the design space one must rely on efficient models that allow the rapid evaluation of the proposed designs and at the same time are able to capture the critical subtleties of the flow. An effective strategy to accomplish these two requirements is the use a multi-fidelity simulation capability. In this paper, we analyze flapping flight for Micro Aerial Vehicle size scales at two different levels of fidelity: an inviscid panel method code (FastAero), and a high-order discontinuous Galerkin method for solving the Navier-Stokes equations (3DG). One of the objectives of this paper is to examine and establish the limits of validity for each approach.

I. Introduction

Flapping flight in nature is a result of many years of refinement and evolution. While a plethora of flapping wing flyers exist in nature, it is difficult to assess the relative importance of flapping parameters (frequency, amplitude, upstroke retraction, forward-aft flapping etc.) and shape characteristics (camber, twist, spanwise bending, etc) by simply experimentally observing and recording the wingbeat kinematics of these animals. For example, while most birds exploit a wing retraction during the upstroke, it is not clear from experimental observations what the importance of such kinematics are, and whether a human designed micro aerial vehicle (MAV) would benefit from mimicking this behavior or whether a related, but different set of bio-inspired wing kinematics would suffice. A compounding factor in the design of flapping MAVs is the large size and complexity of the kinematics design space. Including all possible wing shape variations rapidly results in an intractable problem.

Computation appears to present a possible solution to the flapping design space exploration. It is simple to modify parameters in a computational tool and model or simulate the resulting flapping wing characteristics. Due to the size of the design space, it is unfeasible to consider high-fidelity simulations for each possible flapping configuration. As a result, some reduced order modeling strategy must be leveraged. In our work, we use a modeling strategy that examines variable fidelity physics and geometry representations. The result is a multi-fidelity computational framework[1] that uses potential flow simplifications with differing

*Assistant Professor, Department of Mathematics, University of California, Berkeley, Berkeley CA 94720-3840. E-mail: persson@berkeley.edu. AIAA Member.

†Assistant Professor, Department of Mechanical Engineering, University of Massachusetts, Lowell, Lowell, MA. E-mail: David_Willis@uml.edu. AIAA Member.

‡Professor, Department of Aeronautics and Astronautics, MIT, 77 Massachusetts Avenue 37-451, Cambridge, MA 02139. E-mail: peraire@mit.edu. AIAA Associate Fellow.

geometric representations at the lower fidelity levels, and a high-order Navier-Stokes solution capability at the highest fidelity level. This strategy allows us to use a wake-only strategy[2–4] to sample the vast design space rapidly.[4] The wake only method provides an optimal wake circulation distribution that can be used to design efficient flapping wings and analyze them using a full geometry panel method.[1] The Navier-Stokes simulation capability is then used to refine and verify the lower fidelity computations. This multifidelity method has shown promise in two-dimensions.[5,6]

In this paper we present some initial results comparing a lower fidelity model (potential panel method) with higher fidelity simulations (Navier-Stokes). Here, we consider an analytically described three-dimensional flapping wing and present a small collection of three-dimensional computations. A primary objective of this paper is to understand the limits of validity for each approach. From experimental observations as well as from previous studies[6] we know that efficient designs of interest often involve moderate amounts of flow separation. Therefore it is critical that at the highest fidelity level, viscous effects are modeled accurately.

II. Problem Statement

II.A. Wing Geometry and Flapping Motion

We consider a flapping wing with an elliptical planform. The maximum normalized chord at the wing centerline is $c = 1$ and the wing tip-to-tip span is $b = 10$. The flapping motions occur symmetrically about a hinge located at the wing centerline (see Fig. 1). An HT13 airfoil is selected for the entire wing span, resulting in a maximum wing thickness of $t = 0.065$ at the wing centerline.

We prescribe the symmetric wing motion using a flapping angle at the wing centerline hinge given by

$$\phi(t) = A_\phi \cos 2\pi f t$$

where t is the time, $A_\phi = 30^\circ$ is the flapping amplitude and $f = 1/20$ the flapping frequency. In addition, a wing twist angle is prescribed as a function of the span location. At the distance X from the centerline of the wing, the twist angle is

$$\theta = \frac{X \tan A_\phi}{U + c/2} \sin 2\pi f t$$

with freestream velocity U and chord length c. The resulting flapping motion is illustrated in Fig. II.A. We note that this is not an optimized flapping motion but it is adequate for the purposes of comparing the simulation results obtained with our two different computational models.

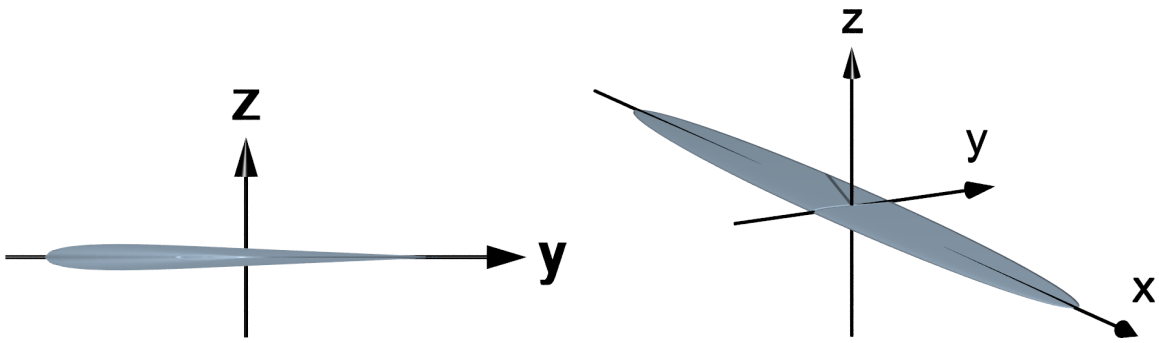

Figure 1. The wing geometry is an elliptic extrusion of an HT13 wing section.

II.B. Flow Properties

The free stream condition corresponds to a 0.1 Mach number flow and for the Navier-Stokes simulations, the chord Reynolds number is 2,000. Computations are carried out at four different incidence angles, $\alpha = 0$, 2.5, 5, and 10.

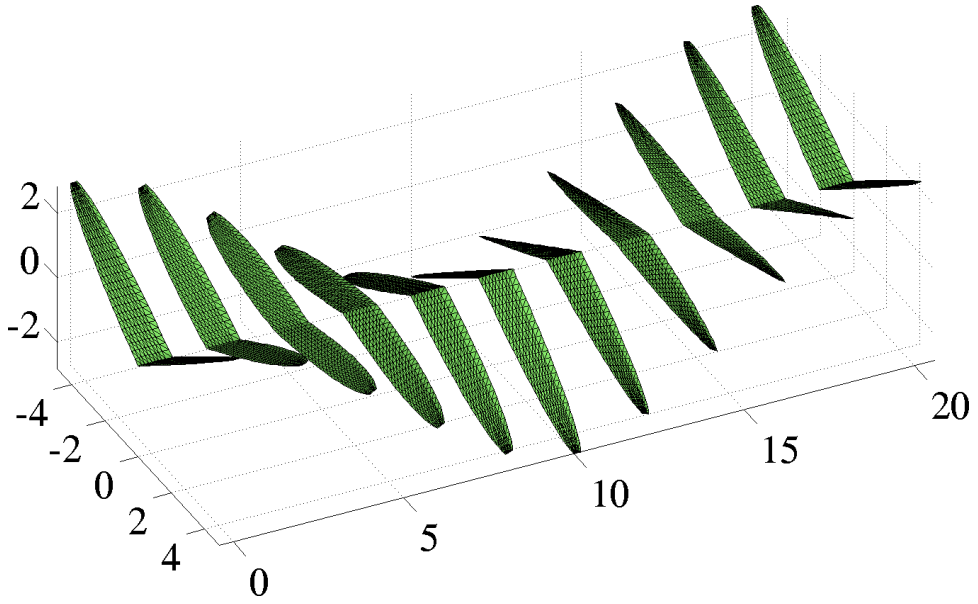

Figure 2. The prescribed flapping motion for the elliptic wing.

III. Computational Models

III.A. Panel Method: FastAero

FastAero[7] is a boundary element or panel method[8–10] for solving potential flow. Panel methods have been used as a very successful aerodynamics design tool for many years. Potential flow panel methods are based on the solution of Laplace's equation written in integral form. Despite the simplifcations introduced by potential flow (inviscid, irrotational, incompressible flow), the methods are powerful and accurate when analyzing the aerodynamic behavior of streamlined shapes. Although, it is possible that flapping wings will experience flow separation, this is not likely to be a desirable operating condition due to the increased energetic demands. As such, it is assumed that birds and bats, as well as engineered vehicles, during regular flight, will not have significant regions of separation.

The three-dimensional version of the FastAero Panel Method[7] is an unsteady, accelerated, panel method with convected vortex particle wakes. The method can be used to model the unsteady potential flow around both thick wings (Dirichlet source-doublet panel method) and thin wings (Neumann doublet panel method). The method uses linear strength basis functions[11] to represent the distribution of source and dipole strength on each of the triangular/quadrilateral elements in the discretization. The method represents the wake vorticity and handles unsteady wake evolution through the use of a vortex particle method.[12–15] The computational cost of the method scales nearly linearly with the number of unknowns in the problem ($\mathcal{O}(n\log(n))$) due to the use of iterative solution methods combined with matrix vector product acceleration. The flapping wing geometry is modeled as an infinitely thin wing and is discretized into triangular panels.

III.B. Discontinuous Galerkin Arbitrary Lagrangian-Eulerian (ALE) Navier-Stokes: 3DG

For the high-fidelity simulations we use the 3DG code,[16–21] which uses high-order accurate discontinuous Galerkin methods to solve the compressible Navier-Stokes equations on unstructured meshes of tetrahedra. High-order methods are advantageous for applications requiring low numerical dispersion and high time accuracy. The DG method produces stable discretizations of the convective operator for any order discretization, thus avoiding the need for additional stabilization or filtering. For the flows considered, high-order methods are capable of fully resolving all the scales present in the flow and hence accurately predict flow separation and reattachment.

The fully unstructured simplex meshes allow for arbitrary geometries and domains, and for efficient adapted meshes that focus the computational resources on relevant regions. To handle the moving boundaries and the deforming domains, we use a mapping-based Arbitrary Lagrangian-Eulerian (ALE) formulation.[22]

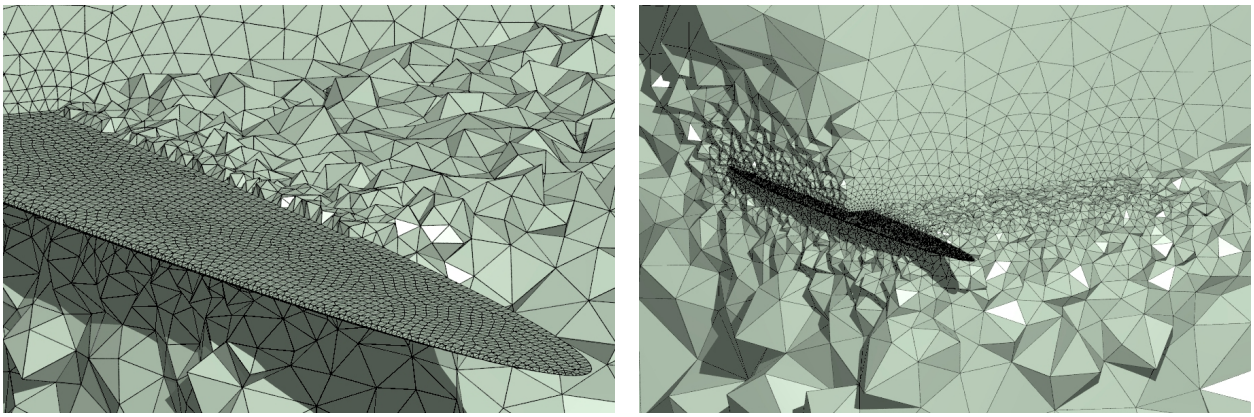

Figure 3. A tetrahedral mesh for the domain around the elliptic wing pair.

III.B.1. High-Order Meshes

In order to obtain maximum geometrical flexibility, the compressible Navier-Stokes equations are discretized on unstructured meshes of triangles and tetrahedra. We use the symmetry of the problem to only simulate one half of the domain, with a symmetry boundary condition at the cut plane. We generate all the surface meshes in parametrized form using the DistMesh triangular mesh generator.[23] The tetrahedral volume mesh is then generated by a Delaunay refinement based code.[24] The resulting mesh has about 30,000 nodes and 160,000 tetrahedral elements for the half-domain. A hand-tuned mesh size function focuses the resolution on the areas around the wings, in particular at the leading and the trailing edges, as well as in the wake. The mesh is shown in Fig. 3.

To obtain truly high-order accuracy, the straight-sided tetrahedral meshes much be modified to account for the curved domain boundaries. We do this using the nonlinear elasticity approach that we proposed in Ref. 25. As a preprocessing step, the layer of elements around the wing is considered to be a deformable elastic solid. Using a nonlinear neo-Hookean model, a well-shaped curved mesh is produced when the facets of the elements in contact with the surface are curved to align with the true geometry.

III.B.2. High-Order Discontinuous Galerkin Discretizations

Our 3DG flow solver is based on the high-order Discontinuous Galerkin (DG) method with tetrahedral mesh elements and nodal basis functions. Here, we use nodal basis functions and cubic polynomials (degree $p = 3$). The viscous terms are discretized using the Compact Discontinuous Galerkin (CDG) method[16] which leads to optimal accuracy, is compact, and generates sparser matrices than the alternative existing methods. The general forms of the system of equations that we solve can be written as

$$\frac{\partial u}{\partial t} + \nabla \cdot F_i(u) - \nabla \cdot F_v(u, q) = S(u, q) \tag{1}$$

$$q = \nabla u, \tag{2}$$

where u is the solution vector, F_i and F_v the inviscid and viscous flux functions, respectively, and $S(u, q)$ the source function. After discretization and elimination of the auxiliary q variables, we obtain a nonlinear system of ordinary differential equations

$$M \frac{dU}{dt} = R(U) \tag{3}$$

with discrete solution vector U, mass matrix M, and nonlinear right-hand side vector $R(U)$. The system of ODEs (3) is integrated in time using a third-order accurate three-stage Diagonally Implicit Runge-Kutta (DIRK) method.[26] This one-step scheme is L-stable, which appears to be a requirement for these types of simulations. Since it is an implicit method, it requires inversion of matrices of the form $M - \alpha \Delta t dR/dU$, where Δt is the timestep and α is a parameter of order one. This is accomplished by using a preconditioned Newton-Krylov technique.

III.B.3. Parallel Newton-Krylov Solvers

The systems of equations produced by the DG discretization are typically very large. We use polynomials of degree $p = 3$, which gives 20 degrees of freedom per tetrahedron and solution component. Since we have 6 solution components, this gives a total number of degrees of freedom around 19 million. In addition, the Jacobian matrices tend to be less sparse than low-order methods, and even though we use an efficient compressed compact storage format,[18] each Jacobian requires has about 7 billion entries, and requires 55GB of storage. It is clear that parallel computers are needed, both for storing this matrices and to perform the computations.

The parallel 3DG code[19] is based on the MPI interface, and we run it on parallel computer clusters. The domain is decomposed using the METIS software,[27] and all discretization and matrix assembly is done in parallel. For the linear solutions, we use an ILU-preconditioned GMRES solver. To maximize the performance of the preconditioner, we order the elements using the Minimum Discarded Fill (MDF) algorithm.[18]

Most of our simulations were done on 16 compute nodes with 8 cores each, or a total of 128 processes. The simulation times in this setting are on the order of 24 hours per 100 timesteps, although this depends highly on the problem, the timestep, and the tolerances in the Newton and the Krylov solvers.

III.B.4. ALE Formulation and Mapping

To account for the moving and the deforming domains, we use the mapping based Arbitrary Lagrangian-Eulerian (ALE) formulation that we proposed in Ref. 22. It requires that the deformations are prescribed either explicitly or indirectly as a mapping $x = x(X, t)$ between the reference and the physical space. On the other hand, it produces solutions of arbitrary orders of accuracy in both space and time. The so-called Geometric Conservation Law is satisfied using an additional equation that is used to compensate for the numerical integration errors.

To obtain a mapping $x = x(X, t)$ for our flapping wing, we use a relatively simple prescribed motion which can be computed and differentiated analytically. In words, the mapping is a shear motion to account for the heaving, another shear motion to account for the wing twist, and a volume-preserving compression/prolongation to ensure the wing length remains the same. The resulting expression is simply

$$x(X,t) = \begin{bmatrix} X\cos\phi \\ Y \\ X\tan\phi + Y\tan\theta + Z\sec\phi, \end{bmatrix} \tag{4}$$

with deformation gradient

$$G = \frac{\partial x}{\partial X} = \begin{bmatrix} \cos\phi & 0 & 0 \\ 0 & 1 & 0 \\ \tan\phi & \tan\theta & \sec\phi. \end{bmatrix} \tag{5}$$

Note that this mapping is volume-presering, since $\det(G) = 1$. The grid velocity $\partial x/\partial X$ is also easily computed analytically.

IV. Results

In our simulations we consider four different freestream angles of attack: $\alpha = 0$, 2.5, 5,and 10 degrees. The wing geometry, frequency, and amplitude are held constant for all simulations.

IV.A. General Description: Potential Flow Simulation Results

Our panel method results provide the time evolution of vertical forces, wing-surface unsteady pressure differential, and wake-surface circulation. Each of these outputs provides insight into the physics of the flow being modeled.

The panel method predicts the time evolved vertical forces shown in Fig. 7. For each incremental angle of attack, we observe the time evolution of the vertical force is similar in shape, but offset in magnitude by a

constant value. This mean-offset is correlated to the incremental change in the angle of attack. This ability to modulate the vertical force by changing the angle of attack suggests a useful strategy for flapping wing flight.

We also use the panel method to compute the unsteady pressure differential across the top and bottom surface of the wing (Fig. 5). The panel method predicts a significant suction peak along the leading edge of the wing that includes a high adverse pressure gradient. Following the initial suction peak in the first quarter chord there is a gradual recovery to a zero pressure differential at the trailing edge of the wing. The large pressure differential spike at the leading edge is characteristic of a potential flow model of thin wings operating at angles of attack. This suction peak is a consequence of the panel method enforcing an attached flow around the sharp leading edge of the wing. In physically relevant flows, leading edge flow separation is likely to occur due to the inability of viscous flows to conform to the curvature of the leading edge.

In potential flow models, the wake vorticity trailing a lifting surface is explicitly modeled. In our panel method the wake is modeled using a vortex particle method; however, in Fig. 4, a-d we show the equivalent time trace of the wake circulation distribution or wake surface potential jump as shed from the trailing edge of the wing. This wake-surface plot illustrates the momentum footprint for the flapping wing and the corresponding wake structure for this wing. Regions of higher circulation magnitude indicate the spatial locations of increased wake circulation and therefore higher wing loading. The vorticity distribution can also be implied from the wake circulation distribution by calculating the tangential gradient of the circulation. Regions of rapid surface-tangential change in the circulation are indicative of increased vorticity distribution magnitude. Circulation contours indicate approximate wake vortex structures in the wake (here a double ladder structure is seen). In this particular wing, we can predict that there is a moderately strong tip vortex, coupled with starting and stopping vortices during each wingbeat cycle.

IV.B. General Description: Navier-Stokes Simulation Results

The results for the Navier-Stokes simulations are shown in Figs. 6–8.

In Fig. 6, entropy iso-surfaces are illustrated in the flow domain, showing regions of flow separation and wake vortex structures. In the lower angle of attack cases ($\alpha = 0$ and 2.5) the flow remains attached for the majority of the wingbeat cycle with only minor regions of separation forming at the mid-to-late downstroke. By contrast, the higher angle of attack cases $\alpha = 5$ and 10 indicate much larger regions of separated flow. This flow separation dominates much of the second half of the downstroke and persists through the first quarter of the upstroke.

The time evolution of the vertical and horizontal forces are shown in Figs. 7–8. The time evolution of the forces correlates with the snapshots of the flow in Fig. 6. During periods of the flapping cycle where the flow remains attached, the lift behaves as expected considering the wing motions. In contrast, when flow separation dominates large spanwise segments of the wing, the force production capability is reduced.

IV.C. Comparison of Results: Effect of Separation on Force Prediction

Our simulation results highlight regimes where potential flow is and is not an adequate approximation of the flow. When flows are characterized by little or no flow separation, they are well approximated by potential flow modelling. For instance, the 0 and 2.5 degree angle of attack cases indicate attached flow for the majority of the wingbeat cycle. We observe some separation bubble development and subsequent mild flow separation during the second half of the downstroke in both of these cases. The corresponding force traces (Fig. 7 a,b) exhibit some mismatch at the points in which viscous effects are present, otherwise good force prediction agreement is observed.

The effects of viscous flow structures are most obvious in the more aggressive 5 and 10 degree angle of attack cases. Due to the low Reynolds number ($\mathrm{Re} = 2,000$), flow separation is difficult to avoid when more aggressive force demands are placed on the lifting surface. At these angles of attack, significant regions of flow separation during the second half of the downstroke are consistently observed. At these points in the flapping cycle, the panel method over-predicts the force generation due to the artificial assumption of fully attached flow; whereas, the Navier-Stokes simulations accurately capture the loss of vertical force due to flow separation. The effects of viscosity are also observed in the first half of the downstroke, where a vortical structure develops and stays over the suction surface of the wing. Before this vortical structure sheds from the wing, there is a rise in the vertical force production, similar to that observed when leading edge vortices are observed in nature.

The simulations confirm the challenges in analyzing and designing effective flapping wings. While our cost effective potential flow method produces accurate results for attached flow cases, it remains only trend relevant once separated flow dominates. While trend relevance is adequate for preliminary design, it may reduce the quality of the wing design if left unchecked. It is therefore critical to accompany any inviscid design predictions with a viscous simulation to confirm the predicted behavior. In essence, this study has confirmed our multi-fidelity approach while also demonstrating the importance of the high fidelity simulations.

In addition the results of the simulations presented here show the importance of wing leading edge geometry. Our panel method predicts a significant leading edge pressure jump and subsequent adverse pressure gradient on the test cases – a strong indication of pending flow separation. In contrast, in related studies, we have observed that the FastAero pressure differential predictions for geometrically accurate bat wings in flight[5] do not have a significant leading edge pressure jump. This is a direct result of the shape of the bat wing's leading edge. In bat flight, the wing-muscle-skeletal system is able to present an aligned or nearly aligned wing leading edge to the flow, thereby reducing the suction peak and likely resulting in a lower susceptibility to leading edge separation. While leading edge angle modulations are not guaranteed to eliminate flow separation, strong consideration of wing shape and subsequent pressure distributions should be made.

IV.D. Acknowledgments

The authors would like to acknowledge the Air Force Office of Scientific Research MURI on biologically inspired flight.

References

[1]Willis, D. J., Israeli, E. R., Persson, P.-O., Drela, M., Peraire, J., Swartz, S. M., and Breuer, K. S., "A Computational Framework for Fluid Structure Interaction in Biologically Inspired Flapping Flight," *18th AIAA Computational Fluid Dynamics Conference, Miami, FL*, June 2007, AIAA-2007-3803.

[2]Hall, K., Pigott, S., and Hall, S., "Power requirements for large-amplitude flapping flight," *JOURNAL OF AIRCRAFT*, Vol. 35, No. 3, MAY-JUN 1998, pp. 352–361, AIAA 35th Aerospace Science Meeting / Nonlinear Dynamical Systems Symposium, RENO, NEVADA, JAN 06-10, 1997.

[3]Willis, D. J., Peraire, J., Drela, M., and White, J. K., "A numerical exploration of parameter dependence in power optimal flapping flight," *24th AIAA Applied Aerodynamics Conference, San Francisco, California*, June 2006, AIAA-2006-2994.

[4]Salehipour, H. and Willis, D. J., "A coupled kinematics and energetics model for flapping flight," *48th AIAA Aerospace Sciences Meeting and Exhibit, Orlando, Florida*, January 2010, AIAA-2010-1229.

[5]Willis, D. J., Israeli, E. R., Persson, P.-O., Drela, M., and Peraire, J., "Multifidelity Approaches for the Computational Analysis and Design of Effective Flapping Wing Vehicles," *46th AIAA Aerospace Sciences Meeting and Exhibit, Reno, Nevada*, January 2008, AIAA-2008-518.

[6]Willis, D. J., Israeli, E. R., and Peraire, J., "Computational Investigation and design of compliant membrane wings for biologically inspired flight vehicles," *Proceedings of ICAS 2008, Anchorage, Alaska*, September 2008.

[7]Willis, D. J., Peraire, J., and White, J. K., "A combined pFFT-multipole tree code, unsteady panel method with vortex particle wakes," *Internat. J. Numer. Methods Fluids*, Vol. 53, No. 8, 2007, pp. 1399–1422.

[8]Hess, J. L., "The problem of three-dimensional lifting flow and its solution by means of surface singularity distribution," *Comput. Methods Appl. Mech. Engrg.*, Vol. 4, 1974, pp. 183–319.

[9]Katz, J. and Plotkin, A., *Low Speed Aerodynamics*, Cambridge University Press, Cambridge, 2001.

[10]Morino, L. and Kuo, C. C., "Subsonic potential aerodynamics for complex configurations: A general theory," *AIAA Journal*, Vol. 12, No. 2, 1974, pp. 191–197.

[11]Newman, J. N., "Distribution of sources and Normal Dipoles Over a Quadrilateral Panel," *J. Engrg. Math.*, Vol. 20, 1985, pp. 113–126.

[12]Leonard, A., "Computing three-dimensional incompressible flows with vortex elements," *Ann. Rev. Fluid Mech.*, Vol. 17, 1985, pp. 523–559.

[13]Gharakhani, A. and Ghoniem, A. F., "Three-dimensional vortex simulation of time dependent incompressible internal viscous flows," *J. Comput. Phys.*, Vol. 134, No. 1, 1997, pp. 75–95.

[14]Rehbach, C., "Calcul numérique d'écoulements tridimenssionnels instationnaires avec nappe tourbillonnaire," *La Recherche Aérospatiale*, Vol. 5, 1977, pp. 289–298.

[15]Voutsinas, S., M.A.Belessis, and Rados, K., "Investigation of the yawed operation of wind turbines by means of a vortex particle method," *AGARD-CP-552 FDP Symposium on Aerodynamics and Aeroacoustics of rotorcraft*, Berlin, Germany, 1995, Paper 11.

[16]Peraire, J. and Persson, P.-O., "The compact discontinuous Galerkin (CDG) method for elliptic problems," *SIAM J. Sci. Comput.*, Vol. 30, No. 4, 2008, pp. 1806–1824.

[17]Persson, P.-O. and Peraire, J., "An Efficient Low Memory Implicit DG Algorithm for Time Dependent Problems," *44th AIAA Aerospace Sciences Meeting and Exhibit, Reno, Nevada*, 2006, AIAA-2006-0113.

[18]Persson, P.-O. and Peraire, J., "Newton-GMRES preconditioning for discontinuous Galerkin discretizations of the Navier-Stokes equations," *SIAM J. Sci. Comput.*, Vol. 30, No. 6, 2008, pp. 2709–2733.

[19]Persson, P.-O., "Scalable Parallel Newton-Krylov Solvers for Discontinuous Galerkin Discretizations," *47th AIAA Aerospace Sciences Meeting and Exhibit, Orlando, Florida*, 2009, AIAA-2009-606.

[20]Persson, P.-O., Peraire, J., and Bonet, J., "A High Order Discontinuous Galerkin Method for Fluid-Structure Interaction," *18th AIAA Computational Fluid Dynamics Conference, Miami, Florida*, 2007, AIAA-2007-4327.

[21]Nguyen, N. C., Persson, P.-O., and Peraire, J., "RANS Solutions Using High Order Discontinuous Galerkin Methods," *45th AIAA Aerospace Sciences Meeting and Exhibit, Reno, Nevada*, 2007, AIAA-2007-914.

[22]Persson, P.-O., Bonet, J., and Peraire, J., "Discontinuous Galerkin Solution of the Navier-Stokes Equations on Deformable Domains," *Comput. Methods Appl. Mech. Engrg.*, Vol. 198, No. 17-20, 2009, pp. 1585–1595.

[23]Persson, P.-O. and Strang, G., "A simple mesh generator in Matlab," *SIAM Rev.*, Vol. 46, No. 2, 2004, pp. 329–345 (electronic).

[24]MORGAN, K. and PERAIRE, J., "Unstructured grid finite element methods for fluid mechanics," *Inst. of Physics Reviews*, Vol. 61, No. 6, 1998, pp. 569–638.

[25]Persson, P.-O. and Peraire, J., "Curved Mesh Generation and Mesh Refinement using Lagrangian Solid Mechanics," *47th AIAA Aerospace Sciences Meeting and Exhibit, Orlando, Florida*, 2009, AIAA-2009-949.

[26]Alexander, R., "Diagonally implicit Runge-Kutta methods for stiff o.d.e.'s," *SIAM J. Numer. Anal.*, Vol. 14, No. 6, 1977, pp. 1006–1021.

[27]Karypis, G. and Kumar, V., "METIS Serial Graph Partitioning and Fill-reducing Matrix Ordering," http://glaros.dtc.umn.edu/gkhome/metis/metis/overview.

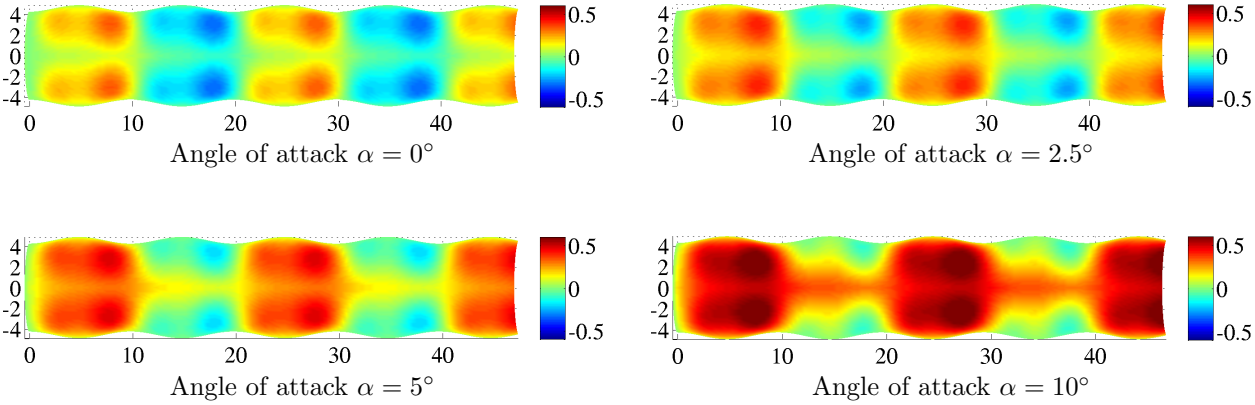

Figure 4. The wake circulation distribution predicted using the panel method is plotted on the surface representing the spatial trace of the wing's trailing edge. The wing is flying from left to right, starting with the downstroke. The wake circulation distribution is an indication of both the momentum transfer to the fluid from the flapping wing and the wake vortex structure.

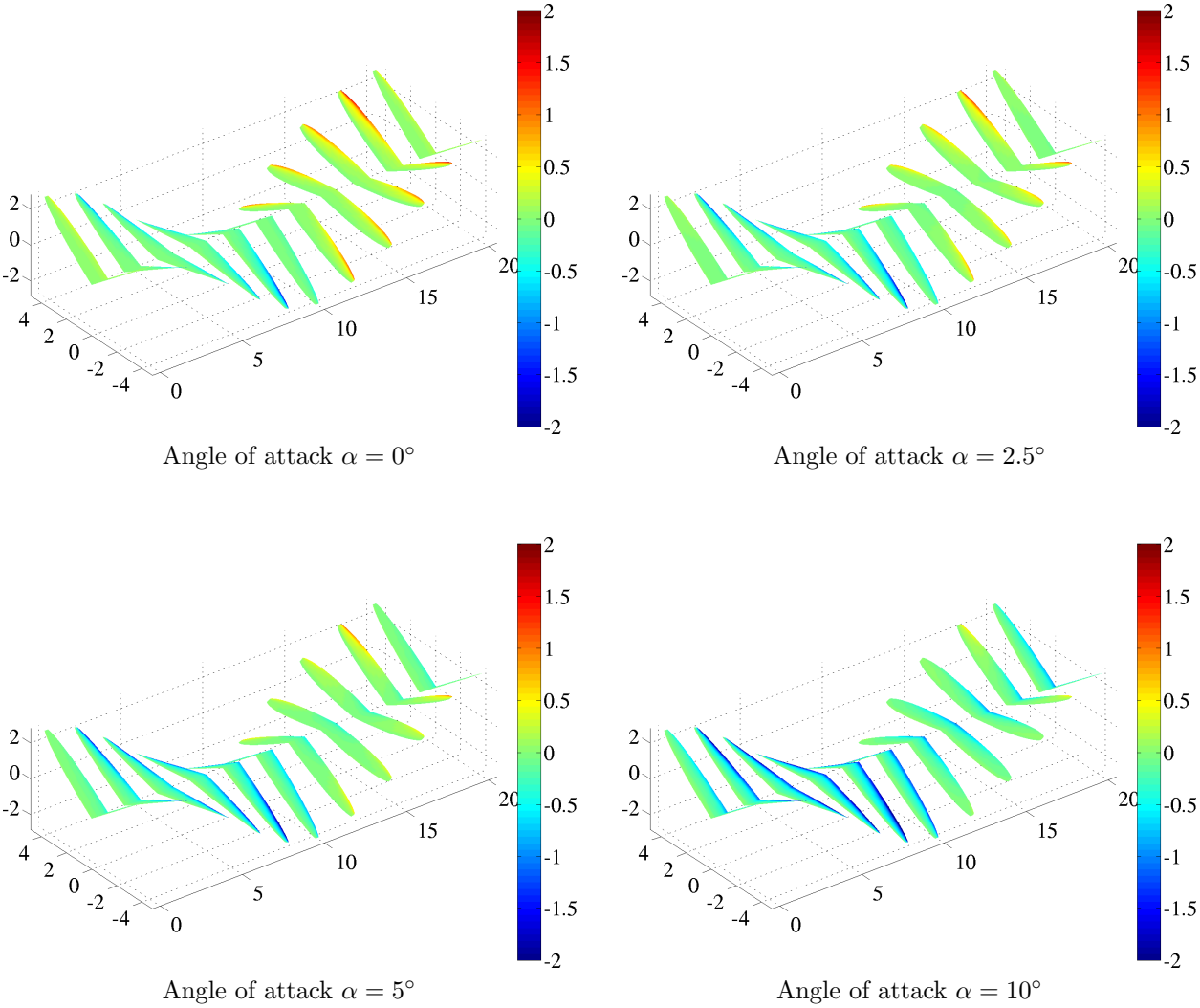

Figure 5. The panel method computed wing surface pressure differential is shown for a series of snapshots during the flapping cycle for each angle of attack. The pressure differential indicates a large pressure differential near the leading edge of the wing, in particular in the outboard locations of the wing.

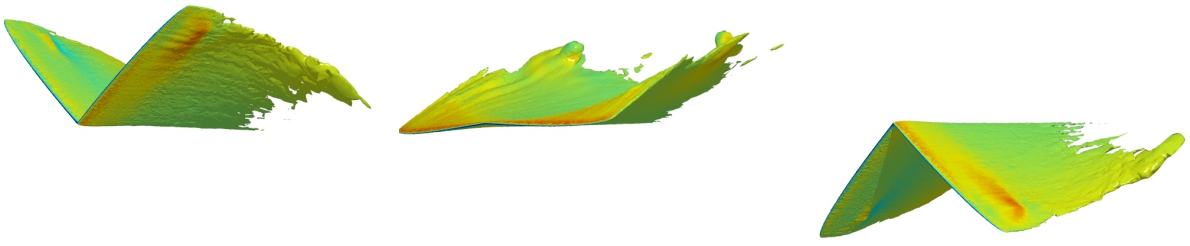

Angle of attack $\alpha = 0°$

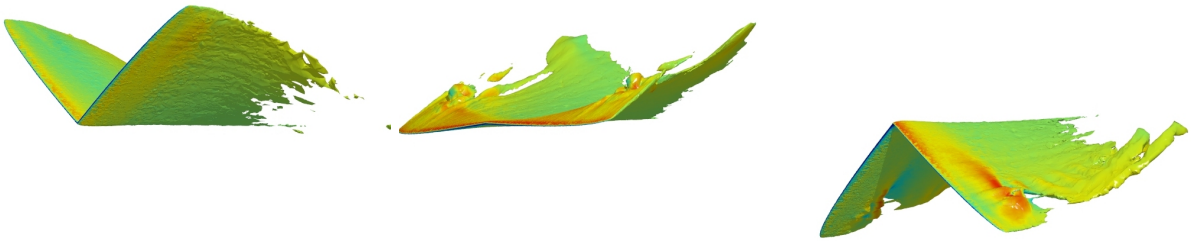

Angle of attack $\alpha = 2.5°$

Angle of attack $\alpha = 5°$

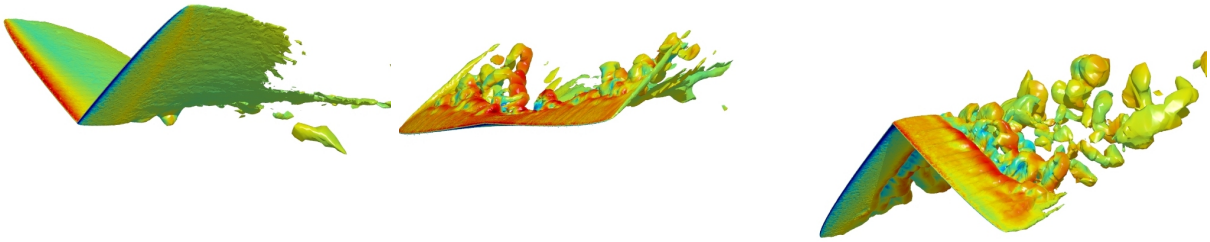

Angle of attack $\alpha = 10°$

Figure 6. The flow field around the flapping wing pair computed by the 3DG Navier-Stokes code, visualized as Mach number color plots on isosurfaces of the entropy. The plots correspond to the four cases of angle of attack (top to bottom) and the times $t = 20$, $t = 25$, and $t = 30$ (left to right).

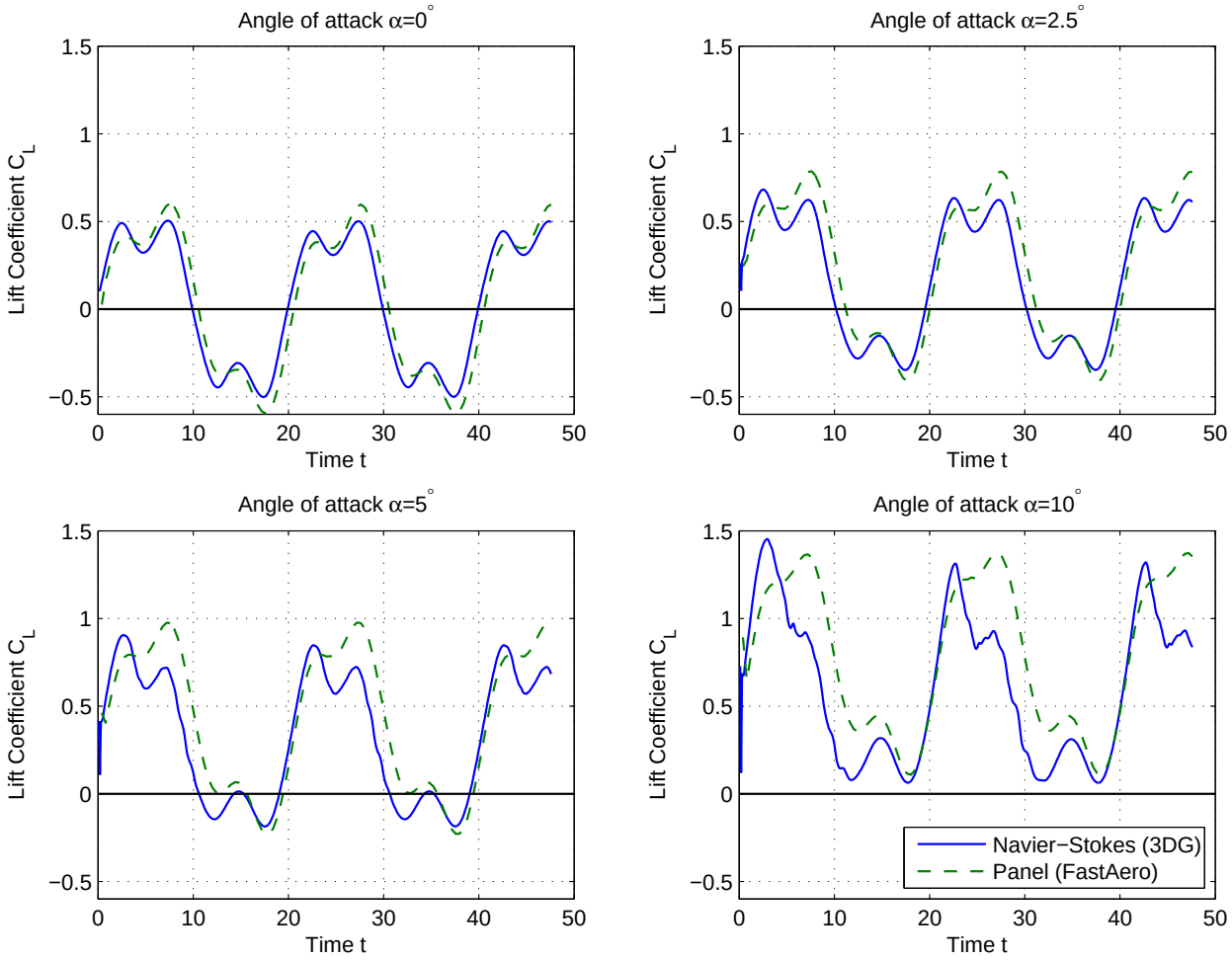

Figure 7. The lift coefficients computed by the two simulation codes for the four cases $\alpha = 0$, 2.5, 5, and 10.

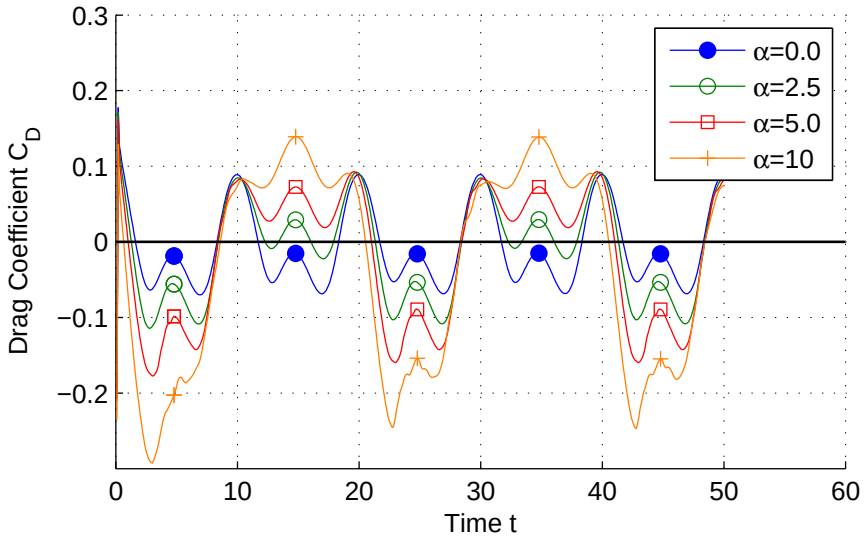

Figure 8. The drag coefficients computed by the Navier-Stokes code (3DG) for the four cases $\alpha = 0$, 2.5, 5, and 10.